

# The global monsoon definition using the difference of local minimum and maximum pentad precipitation rates associated with cross-equatorial flow reversal

Weihong Qian<sup>1</sup> · Ning Jiang<sup>1</sup>

Received: 1 December 2014 / Accepted: 30 March 2015 / Published online: 24 April 2015  
© Springer-Verlag Wien 2015

**Abstract** Since most previous attempts to establish monsoon indices have been limited to specific regions, they have lacked the applicability to universally describe the global monsoon domain. In this paper, we first review the history of global monsoon study and then identify the climatology of global precipitation associated with major systems of the atmospheric general circulation. A new index, based on the annual and semiannual harmonic precipitation rate difference between two local calendar maximal and minimal precipitation pentads, is used to identify the global monsoon domain focusing on where experienced and what caused the climatic dry-wet alteration. The global monsoon domain is defined by the regions where two pentad-mean precipitation difference exceeds  $4 \text{ mm}\cdot\text{day}^{-1}$ , which is also influenced by the low-level prevailing wind reversal associated with the cross-equatorial flow. This definition not only confirmed previous results of the classical global monsoon domain from the tropical Africa to Asia-Australia and non-classical monsoon region in the tropical America but also solved an issue of missing local summer monsoon spots.

## 1 Introduction

There are different viewpoints explaining the causes of monsoon (Chao and Chen 2001). Globally, the solar

radiation and the land-ocean distributions were considered as the first two primary driving forces for the formation of the global monsoon (Ramage 1971; Webster 1981, 1987; Zeng and Li 2002). Two of the most important early studies were done in the late seventeenth and early eighteenth centuries by Edmund Halley and George Hadley (Webster 1981). Halley attributed the monsoon circulation primarily to differential heating and cooling of the land and the ocean. Differential heating would cause pressure differences in the atmosphere that would be equalized by winds. Hadley noted that the rotation of the earth would change the direction of such winds, causing winds moving toward the Equator to veer to the right in the Northern Hemisphere (NH) and to the left in the Southern Hemisphere (SH). Wang et al. (2012) indicated that the annual variation of solar radiation is a fundamental driver and a necessary and sufficient condition for the existence of monsoon, while the land-sea thermal contrast is critical for the location and strength of the monsoon but it is neither a necessary nor a sufficient condition. In fact, however, wind reversal, besides heating contrast, also involves in monsoon formation. Thermal contrast, due to variation of solar radiation and the land-sea distributions, causes wind direction reversal, which changes the locations of the wind convergence in the lower troposphere, and as a result, forming regional dry-wet alteration. Thus, the physical mechanism of monsoon, in short, should be thermal contrast changing wind field and hence causing dry-wet alteration.

Although the term of global monsoon domain has been proposed in many previous works using different indices, debates on whether such a global domain can be objectively determined still remain, as summarized by Wang and Wu et al. (2008) and indicated recently by Nguyen et al. (2014). By an annual precipitation range between local summer and winter, Wang and Ding (2008) depicted a global monsoon

---

✉ Ning Jiang  
jiangningjxxgch@sina.com

Weihong Qian  
qianwh@pku.edu.cn

<sup>1</sup> Department of Atmospheric and Oceanic Sciences,  
Peking University, Beijing 100871, China

domain. However, as Nguyen et al. (2014) indicated, some “spots” could not be detected by their definitions due to the use of a local calendar rainfall or zonal wind threshold with the difference between two calendar seasons of local summer and winter. This is a critical issue concerned by climatologists and short-term climate forecasters. In recent years, paleo-monsoon studies are carried out by geologists (e.g., Liu et al. 2004; Wang 2009; Wang et al. 2009). However, it is necessary to know if a proxy series, such as from stalagmite records or lake/sea sediments, is located at an identified monsoon region or not. For the climate change, the global and regional monsoon simulation is a new field (Liu et al. 2009; Kim et al. 2008; Sperber et al. 2013; Song et al. 2014). The simulated and projected results for the past or the future century climate should be compared with observations. In routine practice, seasonal drought and flood predictions in many Asian countries are focused on different monsoon regions (Barlow et al. 2002; Tippett et al. 2005; Chu et al. 2008). Thus, these issues concerning some spots need to be resolved by a new monsoon definition.

To find out how many monsoon regions existing in the world, we need first to have an objective definition and then an objective division for the global monsoon. In this paper, we give a new definition of the global monsoon by combining several previous studies. Datasets and methodology are described in Section 3, after a history review of global monsoon study in Section 2. We systematically identify where climatologically experiences dry-wet alteration from global precipitation in Section 4. The closely relation of the dry-wet alteration associated with local wind reversal is identified in Section 5. Finally, the global monsoon domain satisfying dry-wet alteration associated with the low-level cross-equatorial prevailing winds is summarized in Section 6.

## 2 Review of history

The earliest worldwide monsoon description was given by Khromov (1957), who used the annual frequency of surface wind reversal to categorize three types of monsoon: the first is from East Africa to South Asia and Southeast Asia as well as the equatorial western Africa; the second covers the equatorial Africa, East Asia-Northwest (NW) Pacific, the maritime continents, and other local areas; the third is located in mid-high latitudes. Later, Ramage (1971) mapped a worldwide monsoon including the first two types of Khromov’s description. The great progress on worldwide monsoon was made by Webster (1987) who combined prevailing wind reversal and dry-wet alteration between winter and summer and mapped six monsoon regions in the whole world.

Prior to this century, many works focused on the study of regional-scale monsoon variations, mostly on continents over South Asia or Indian Continent (e.g., Lau and Yang 1997; Webster et al. 1998; Wang and Fan 1999), East Asia (e.g., Tao and Chen 1987; Chen and Zhu et al. 1991), Australia (e.g., McBride 1987), Africa (e.g., Nicholson and Kim 1997), South America (e.g., Zhou and Lau 1998), and North America (e.g., Adams and Comrie 1997), but very few on the global monsoon. This is because observed precipitation is not available in many places over ocean.

Since satellites provide a global observation in late 1970s, some products such as the outgoing long-wave radiation (OLR) and the upper tropospheric water vapor band brightness temperature (BT) can be used in the worldwide monsoon study. Using the OLR and highly reflective clouds, Wang (1994) delineated the global tropical monsoon regimes. The term of “global monsoon” (GM) first appeared in the work of Sankar-Rao (1966, 1969), but he did not give any precipitation (or dry-wet change) and wind descriptions except a set of equations of atmospheric motion. The term of GM used in dry-wet alteration from the global scale was first found in the literature of the late twentieth century by using BT product (Qian et al. 1998a, 1998b). Globally, six major monsoon regions in North-South Africa, Asia-Australia, and South-North America were revealed by the analyses of OLR (Wang 1994) and BT (Qian 2000) despite the differences existed in their coverages. Two years later, Trenberth et al. (2000) depicted the GM as the global scale seasonally varying overturning circulation throughout the tropics. Meanwhile, Qian (2000) described the GM by dry-wet alternation in the global scale using monthly-mean BT satellite data. To determine the GM, Qian et al. (2002a) used the NCEP/NCAR 850 hPa reanalysis wind and BT to summarize the GM distribution based on the analysis of both dry-wet alteration and wind reversal associated with the cross-equatorial flow. From the GM (Qian et al. 1998a, 1998b; Qian 2000; Qian et al. 2002a) and some regional monsoons in Asia (Qian and Yang 2000; Qian and Lee 2000), the summer monsoon in the subtropics was defined as the expansions of three deep convective centers or three wet centers in the equatorial region, driving through low-level cross-equatorial flow. The largest deep convective center (or wet center) is located in the equatorial maritime continents and the other two in the equatorial America and the equatorial Africa. The geographical distribution of the GMs, including the tropical, subtropical, and temperate-frigid monsoons, was pictured by Li and Zeng (2002) using the normalized seasonality of wind field. Zeng and Lu (2004) depicted the onset and retreat of GM using the normalized precipitable water data. Using the Global Precipitation Climatology Project (GPCP) data, Wang and Ding (2006) as well as Zhang and Wang (2008) illustrated

the GM domain, defined by the difference between varied seasonal mean precipitation rates from local summer season in the NH and winter season in the SH. Furthermore, Wang and Ding (2008) as well as Zhang and Wang (2008) demonstrated that the GM represents the dominant mode of the annual variation of the tropical precipitation and low-level winds. Considering the relationship between the GM and general circulation systems, Qian and Tang (2010) compared the GM troughs and global atmospheric centers of action in the two calendar pentads 8 and 44.

The existing worldwide monsoon or GM studies can be classified into three categories. The first studies the prevailing wind reversal such as those made by Khromiv (1957), Ramage (1971), Trenberth et al. (2000) and Li and Zeng (2003). For the first category, prevailing wind reversals detected do not only exist in the subtropical areas but also in the equatorial zone and mid-high latitudes. The second is the dry-wet alteration, studied by Wang (1994), Qian et al. (1998a, 1998b), Qian (2000), Zeng and Lu (2004), and Wang and Ding (2006). In this category, three datasets of OLR, BT, and precipitable water downloaded from satellites can roughly describe the GM domains. The last category combines dry-wet alteration and prevailing wind reversal, such as from the studies of Webster (1987), Qian et al. (2002a), Wang and Ding (2008), Zhang and Wang (2008), and Qian and Tang (2010). As indicated recently by Nguyen et al. (2014), some “spots” could not be detected by some definitions used local rainfall or zonal wind threshold of local difference between two calendar seasons of summer and winter. A spot in southern China also exists in our previous study using a rainfall of local precipitation difference between two calendar pentads 8 and 44 (Qian and Tang 2010). The limitation is, indeed, because the studies only put dry-wet alteration and prevailing wind reversal together without explicitly establishing a unified index to picture the GM. The two determined calendar seasons or pentads are not suitable to distinguish where the monsoon regions are, because the climatic maximal and minimal precipitation rates are asymmetrically seasonal advance from a place to another. For example, different dry-wet alterations can be found in adjacent small regions over Southeast Asia (Qian and Yang 2000).

### 3 Datasets and methodology

Two datasets are used in this study. The first is the daily-mean NCEP/NCAR Reanalysis data (NCEP R2) from 1979 to 2013 (Kanamitsu et al. 2002) downloaded from the website (<http://www.esrl.noaa.gov/psd/data/gridded/data.ncep.reanalysis.html>) with a horizontal  $2.5^\circ$  longitude-latitude grid interval and 17 vertical levels. In this paper, winds

at 850 hPa are used to describe the change in wind direction because moisture and heat transports are mainly concentrated near the low-level jet streams. The second is the Climate Prediction Center (CPC) Merged Analysis of Precipitation (CMAP) derived by merging rain gauge observations, five satellite estimates, and numerical model outputs from the website ([http://www.cpc.ncep.noaa.gov/products/global\\_precip/html/wpage.cmap.html](http://www.cpc.ncep.noaa.gov/products/global_precip/html/wpage.cmap.html)) with a horizontal  $2.5^\circ$  longitude-latitude grid interval for 1979–2011 (Xie and Arkin 1997).

An atmospheric total field  $F_d(\lambda, \varphi, p, t)$  such as geopotential height, temperature, and zonal (meridional) wind on calendar day  $d$  (CMAP precipitation on calendar pentad) in year  $y$  at a spatial point of pressure level  $p$ , longitude  $\lambda$  and latitude  $\varphi$ , can be decomposed into a climatic field  $\tilde{F}_d(\lambda, \varphi, p)$  and an anomalous field  $F'_d(\lambda, \varphi, p, t)$  used in our recent studies (Qian and Jiang 2014; Qian et al. 2015):

$$F_d(\lambda, \varphi, p, t) = \tilde{F}_d(\lambda, \varphi, p) + F'_d(\lambda, \varphi, p, t) \quad (1)$$

The climatic field is estimated by averaging  $M$  ( $\geq 30$ ) years based on the reanalysis data or other datasets on a calendar day  $d$ ,

$$\tilde{F}_d(\lambda, \varphi, p) = \sum_{t=1}^M F_d(\lambda, \varphi, p, t) / M \quad (2)$$

It is assumed that the positive and negative anomalies of meteorological variables at a specific grid point and a given calendar day cancel each other during the  $M$  year period to approximate the quasi-static climatic state.  $M$  is taken from 1981 to 2010 for the CMAP precipitation and for the NCEP R2. Thus, as an example, when  $d$  is set on 1st May,  $t$  is days from 1st May 1981, 1st May 1982, ..., 1st May 2010 for  $M$  years.

To obtain a smoother day-to-day climatology of atmospheric variables, a Fourier analysis is performed at each of all grids for a 365 day or 73 pentad series a year. The method of extracting the annual and semi-annual harmonics is derived from the website (<http://www.ncl.ucar.edu/Document/Functions/Contributed/smithClimDayTLL.shtml>). Finally, a smooth climatic cycle contains only annual and semiannual components while all harmonics greater than 2 are set to zero. This method is reasonable in the tropical and subtropical zones to find the seasonal maximum and minimum precipitation rates which are mainly caused by the solar maximum radiation crossing the equator twice a year.

The absolute criterion of  $4 \text{ mm}\cdot\text{day}^{-1}$  was used in our previous summer monsoon studies and compared with  $5 \text{ mm}\cdot\text{day}^{-1}$  and  $6 \text{ mm}\cdot\text{day}^{-1}$  thresholds from regions of the South China Sea (SCS) (Qian and Yang 2000), East Asia (Qian et al. 2002a), South Asia (Qian and Zhu 2002),

Asia-Australia (Tang and Qian 2009), to the global monsoon (Qian and Tang 2010), as well as to identify the northernmost boundary of East Asian summer monsoon (Hu and Qian 2007; Qian et al. 2007; Qian et al. 2009). From these studies, we noted that the absolute criterion of  $4 \text{ mm}\cdot\text{day}^{-1}$  can be used in the tropical monsoon definition such as the climatic rapid onset of the central SCS summer monsoon with the precipitation rate from  $2 \text{ mm}\cdot\text{day}^{-1}$  in April to more than  $6 \text{ mm}\cdot\text{day}^{-1}$  in middle May and also used in the identification and interannual-interdecadal studies of subtropical monsoon in northern China and even in Australia in the SH. In the present study, we use a relative criterion of  $4 \text{ mm}\cdot\text{day}^{-1}$ .

#### 4 Where does a dry-wet alteration exist?

One could imagine that if the entire earth is covered by water and solar rays always radiate on the equatorial zone without seasonal variation, there should be only three large precipitation zones caused by, respectively, a trade flow convergence along the equator and two polar frontal convergences near  $60^\circ$  latitudes. The three large precipitation zones are also corresponding with the convergence of two Hadley cells in tropics and the convergences between the Ferrel and Polar cells in the two middle latitudes. In this situation, dry-wet alteration and wind reversal cannot be observed in the global scale. For another situation, if seasonal and meridional variations of solar radiation are considered, there should be dry-wet alteration and prevailing wind reversal caused by location shifts of the inter-tropical convergence zone (ITCZ) and two polar frontal convergence zones. There are two subtropical dry zones under the two subtropical high zones. The tropical GM can be identified from either or both of the dry-wet alteration and wind-direction reversal associated with the low-level cross-equatorial flow in the tropics. Other two zones in the middle latitudes also satisfy dry-wet alteration but wind-direction reversal is not associated with the low-level cross-equatorial flow. Thus, whether the dry-wet alteration is associated with cross-equatorial flow becomes a critical condition to define monsoon regions.

However, the earth surface is covered by multi-scale oceans and continents, which form various circulation systems. The intensity change and location shift of these systems are influenced by solar seasonal radiation and sea-land distributions. The ideal two subtropical high zones become five subtropical high centers in three oceans (Fig. 1a). Globally, large portion of precipitation falls in oceans (Fig. 1a). Over continents, two major large precipitation regions are located in the two tropical rain forests of equatorial South America and equatorial western Africa. In the longitudes of Atlantic and the Americas, the two mid-latitude

precipitation centers of c1 and b1 are caused by subtropical highs and mid-latitude westerly flows, the precipitation region d1 is formed at the inter-tropical convergence zone (ITCZ), and the precipitation center a1 is formed between two neighbor SH subtropical highs in the Atlantic and Pacific. The same pattern but stronger highs and mid-latitude westerly flows is also noted in the mid-low latitudes of Pacific for the four precipitation centers or regions (a2, b2, c2, and d2). The similar pattern of the three precipitation regions or centers (a3, b3, and d3) is surrounded the subtropical high in the Indian. From the three ideal global precipitation zones to the 13 precipitation centers or regions in Fig. 1a, regional or local precipitation can be explained by different circulation systems. The three precipitation regions d1, d2, and d3 near the equatorial zone are caused by the ideal ITCZ. The five precipitation regions b1, b2, and b3 in the SH as well as c1 and c2 in the NH are caused by the mid-latitude westerly flows and the subtropical highs. However, the four precipitation centers a1, a2, a3, and a4 are caused by the large-scale sea-land (topography) contrast and five subtropical highs. It is clear that the global monsoon precipitation is directly associated with the intensity variability and location shift of seven precipitation centers (a1, a2, a3, a4, d1, d2, and d3). Climatologically, the location of three precipitation regions d1, d2, and d3 shifted off the equatorial zone is due to the asymmetry of large-scale sea-land distribution in the two hemispheres while the formation of other ten precipitation centers is mainly attributed to the zonally oriented large-scale sea-land distributions and subtropical highs.

If only the maximal pentad precipitation rate of the smooth climatic cycle from annual and semi-annual harmonic components is concerned, the large-scale structure is similar to that of annual-mean precipitation rate except for the complexity found in the Eastern Hemisphere, particularly over the region between Asia and Australia (Fig. 1b). From Asia to NW Pacific, there are five centers of maximal pentad-mean precipitation rate, respectively, in the Arabian Sea, the BOB, the SCS, the east sea of the Philippines, and the subtropical NW Pacific. In East Asia, the precipitation rate of  $4 \text{ mm}\cdot\text{day}^{-1}$  can reach Northeast China ( $130^\circ \text{ E}$ ,  $50^\circ \text{ N}$ ). In the subtropical SH, there are four centers of pentad-mean precipitation rate, respectively, in the Madagascar Island, the south of equatorial-central Indian Ocean, the Arafura Sea, and the Solomon Islands. The most prominent feature shows that these centers of maximal pentad-mean precipitation rate are located in off-equatorial zones. As a comparison, the global distribution of minimal pentad-mean precipitation rate is shown in Fig. 1c, where the center of exceeding  $4 \text{ mm}\cdot\text{day}^{-1}$  is located from the equatorial eastern Indian Ocean and the equatorial western Pacific.

After illustrating the climatic pentad-mean precipitation intensity, Fig. 2 shows the climatic precipitation

**Fig. 1** Global climatic distribution of **a** annual-mean precipitation rate (shading,  $2 \text{ mm}\cdot\text{day}^{-1}$  interval) and wind arrow ( $\text{m}\cdot\text{s}^{-1}$ ) at 850 hPa, **b** maximal pentad-mean precipitation rate ( $2 \text{ mm}\cdot\text{day}^{-1}$  interval), and **c** minimal pentad-mean precipitation rate ( $2 \text{ mm}\cdot\text{day}^{-1}$  interval). In **a**, the *thick red line* denotes subtropical high (anticyclone) ridge while the *thick black-dashed line* is along the axis of precipitation rate, *letter "A"* denotes the location of anticyclone at 850 hPa, *letters "a", "b", "c," and "d"* indicate precipitation axes. In **b**, the *heavy dashed lines* denote the axes of precipitation rate

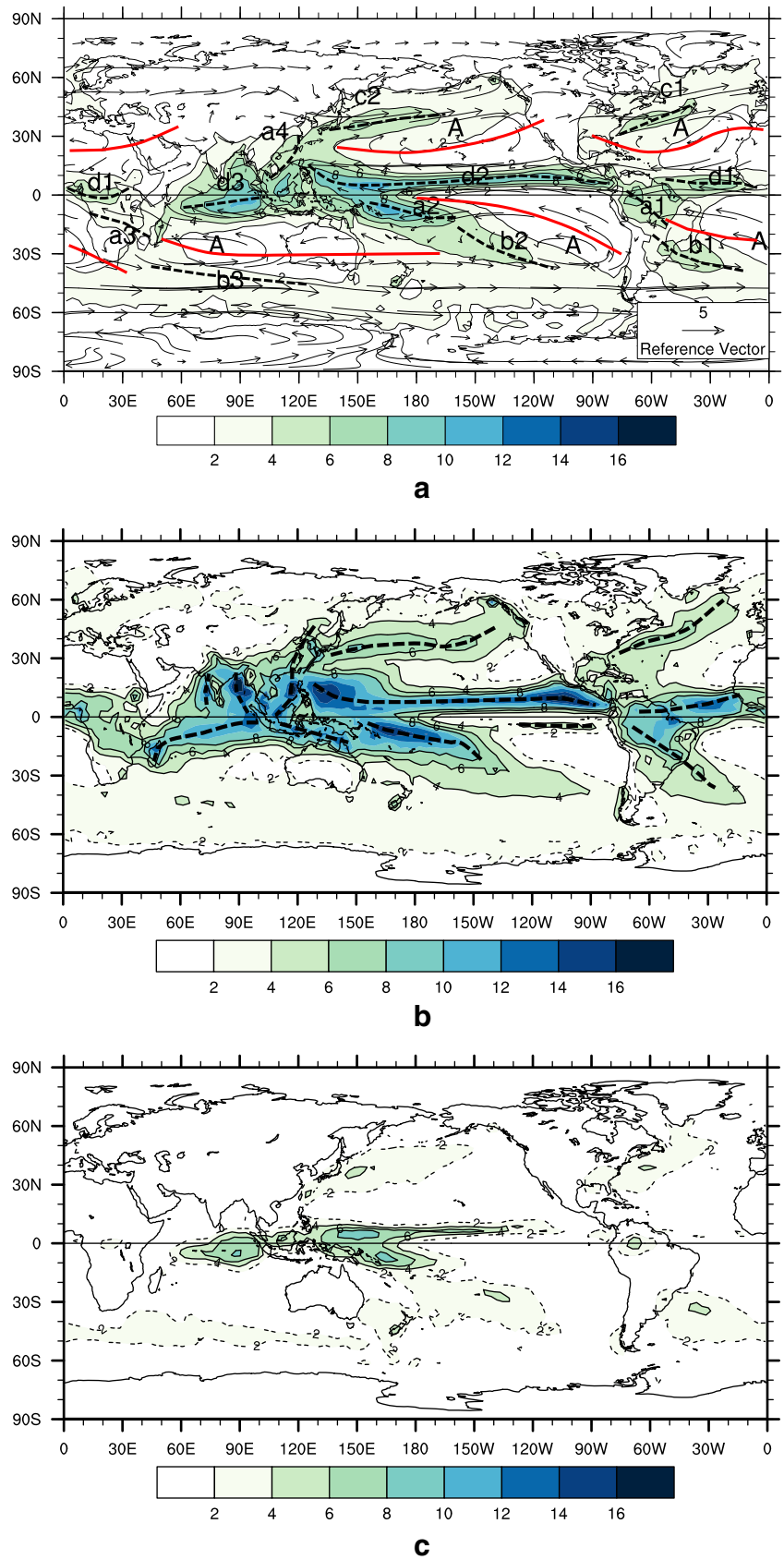
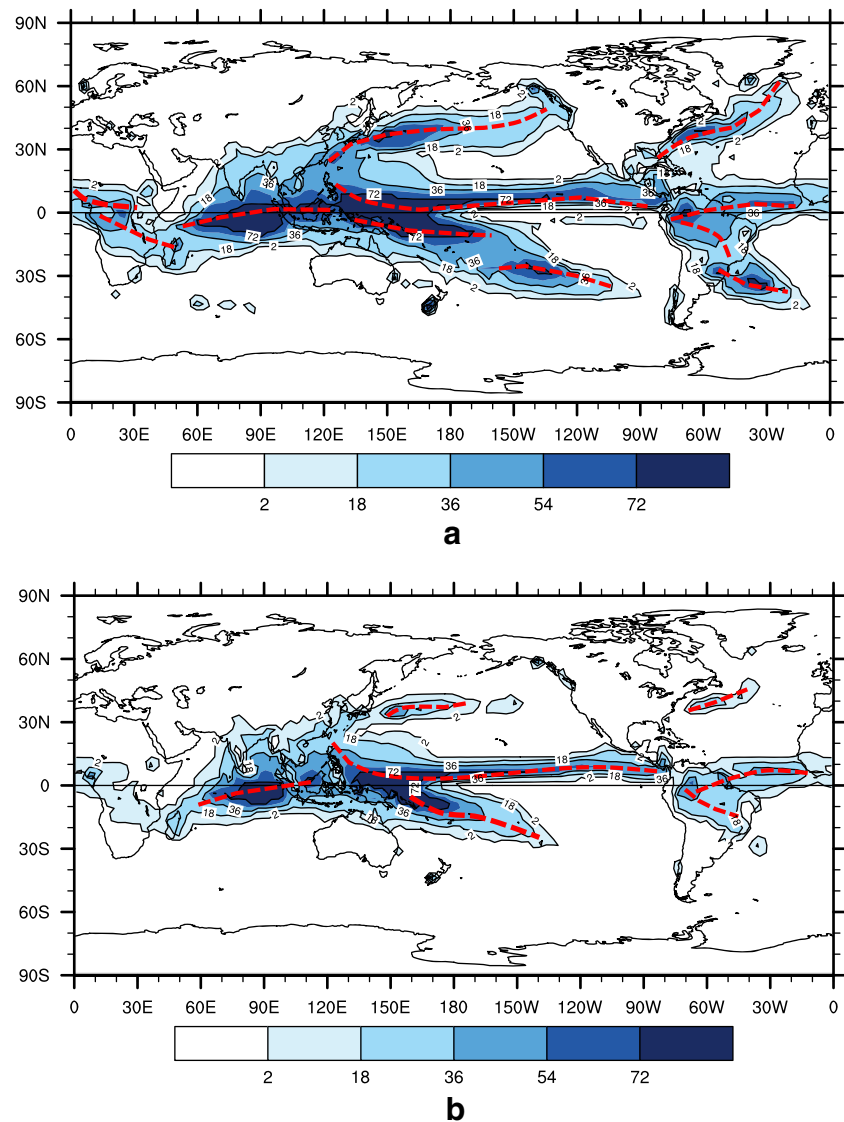


**Fig. 2** Climatic precipitation durations (pentads) with precipitation rate exceeding **a**  $4 \text{ mm}\cdot\text{day}^{-1}$  and **b**  $6 \text{ mm}\cdot\text{day}^{-1}$ . The red dashed line is along the high number of pentads



durations with precipitation rate exceeding 4 and  $6 \text{ mm}\cdot\text{day}^{-1}$  worldwide, respectively. We first examine the duration with precipitation rate exceeding  $4 \text{ mm}\cdot\text{day}^{-1}$  in Fig. 2a. In equatorial Indian Ocean and equatorial western Pacific, there are two regions with the longest precipitation duration (72–73 pentads). It means that there is no climatic dry spell or no climatic dry-wet alteration whole year. Wet spell centers with durations longer than half a year (36 pentads) can be observed in subtropics of NW Pacific, NW Atlantic, central southern Pacific, and Southwest Atlantic. These centers are mostly located over open oceans. Over continents, two centers of precipitation duration more than 36 pentads are found in equatorial western Africa and tropical South America. In the Asia continent, the duration is less than 36 pentads.

We then compare the duration with precipitation rate exceeding  $6 \text{ mm}\cdot\text{day}^{-1}$  in Fig. 2b. The distribution is similar

to that with  $4 \text{ mm}\cdot\text{day}^{-1}$ . Two duration centers of precipitation rate exceeding  $6 \text{ mm}\cdot\text{day}^{-1}$  are still found in equatorial Indian Ocean and equatorial western Pacific. Over continents, the largest area with the precipitation duration longer than 18 pentads (three months) is observed in tropical South America. In the Asia continent, the region with three-month duration is found near the BOB, over the ICP, and the southern China coast. If taking the precipitation rate more than only  $3 \text{ mm}\cdot\text{day}^{-1}$ , the coverage of the climatic precipitation duration is larger than that in Fig. 2a such as in eastern China and North America.

Various definitions using different indices for the GM have been proposed in the last decade (e.g., Qian et al. 1998a; Trenberth et al. 2000; Qian 2000; Li and Zeng 2002; Qian et al. 2002a; Wang and Ding 2006, 2008; Zhang and Wang 2008). Figures 1 and 2 cannot tell where a tropical monsoon region is because one of monsoon

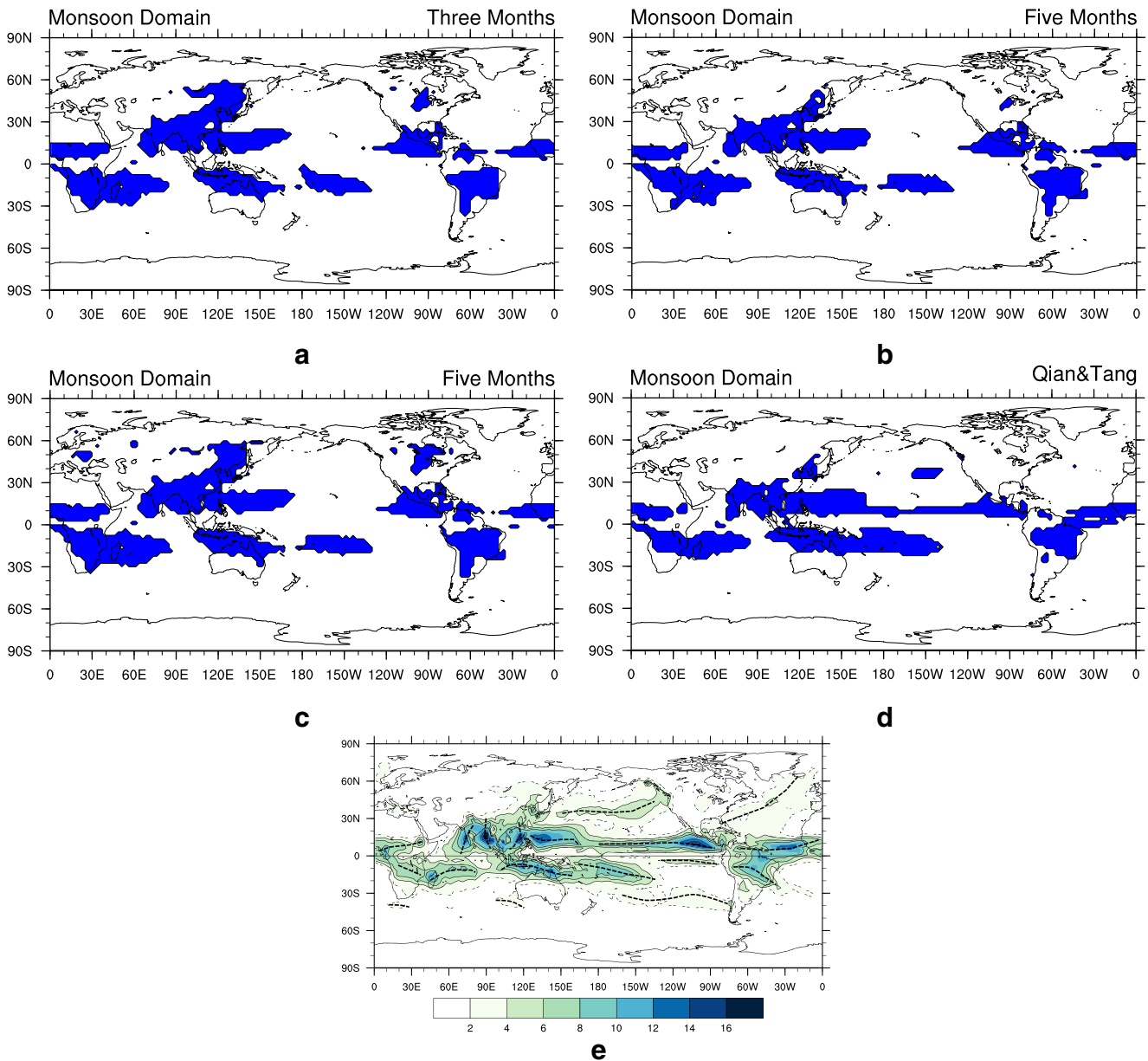


**Fig. 3** Five global monsoon precipitation domains (shading) defined by **a** Wang and Ding (2006), **b** Zhang and Wang (2008), **c** Wang et al. (2014), **d** Qian and Tang (2010), and **e** this paper. From **a** to **d**, their definitions are described in

the text. In **e**, climatic difference ( $2 \text{ mm}\cdot\text{day}^{-1}$  interval) of global maximal and minimal pentad-mean precipitation rates with the *heavy dashed lines* denoting the axes of precipitation rate difference

definitions is seasonally dry-wet alteration. Using the global precipitation datasets, Wang and his coauthors have given different thresholds to depict the GM domain. Figure 3a is the global monsoon precipitation domain defined by the region in which the local annual range (AR) intensity using the local summer (JJA)-minus-winter (DJF) precipitation exceeds 180 mm and the local summer monsoon precipitation exceeds 35 % of annual rainfall (Wang and Ding 2006). Some spots such as in South China, from the East China Sea to south of Japan, and the western SCS can be found.

In the middle latitudes such as the Northeast Asia beyond  $50^\circ \text{ N}$  and the central North America are located in the monsoon regions. Figure 3b shows the summer monsoon rainy season domains, where the summer 5-month rainfall (MJJAS for the NH, NDJFM for the SH) is equal to or above  $3 \text{ mm}\cdot\text{day}^{-1}$ , and the ratio of summer to annual rainfall is greater than 55 % (Zhang and Wang 2008). The coverage of GM domain mapped by Zhang and Wang (2008) is smaller than that mapped by Wang and Ding (2006) but some spots indicated by Nguyen et al. (2014) still existed. Recently, a

new proposed global monsoon domain satisfies (1) the local summer (MJJAS)-minus-winter (NDJFM) precipitation rate exceeds  $2 \text{ mm}\cdot\text{day}^{-1}$  and (2) the local summer precipitation exceeds 55 % of the annual total (Wang et al. 2014). This is a set of relaxed condition so that the coverage becomes larger than that in Figs. 3a, b particularly in Europe, North-east Asia, and North America, but those spots still remained. In our previous study, the difference of pentad-mean precipitation rate between pentad 8 and 44 was used to detect the tropical GM domain (Qian and Tang 2010). Six monsoon regions are clearly observed off the equatorial zone but some spots also existed (Fig. 3d). All these definitions cannot eliminate some spots such as in southern China where a stationary frontal precipitation is often active from spring season to early summer (Zhang and Wang 2008; Zhao et al. 2009; Zhu et al. 2011).

Regarding the fact that the summer wet spell is shorter than 1 month in many subtropical regions and taking climatic annual and semiannual cycles, Fig. 3e shows the climatic difference between maximal and minimal climatic pentad-mean precipitation rates of every grid in the world, which eliminates the spots mentioned above. Along the equatorial zone, many places do not reach the threshold of  $4 \text{ mm}\cdot\text{day}^{-1}$  difference except only three equatorial lands in western Africa, the maritime continents, and tropical South America. These three areas also have relative dry spell as shown in Fig. 1b. Comparing to the tropical GM domain of Wang and Ding (2006, 2008), the domain of  $4 \text{ mm}\cdot\text{day}^{-1}$  difference covers a larger area but that of  $6 \text{ mm}\cdot\text{day}^{-1}$  difference misses some places such as that in East Asia. Figure 3e tells where experiences dry-wet alteration worldwide but it depends on thresholds such as 4 or  $6 \text{ mm}\cdot\text{day}^{-1}$ . If taking  $2 \text{ mm}\cdot\text{day}^{-1}$  as threshold, regions of dry-wet alteration can be observed in middle latitudes as indicated by the thin dotted lines in Fig. 3e.

Figures 4a, b, respectively, show the two calendar pentads when the precipitation rate climatologically reaches the maximum and minimum in the world. But we here only focus on the regions satisfying the above condition of dry-wet alteration (the difference between two pentad-mean precipitation rates exceeds  $4 \text{ mm}\cdot\text{day}^{-1}$  or covered by white lines). In the subtropical SH (Fig. 4a), the maximal precipitation pentad is concentrated in the austral summer (from pentads 70 to 15). The complexity is observed in NH and along the equatorial zone. In the equatorial western and eastern Africa, maximal precipitations are from pentads 60 to 70 and from pentads 20 to 30, respectively. In the maritime continents, maximal precipitation pentads are from 60 to 73. The maximal precipitation in the eastern BOB appears in pentads 30–40 while the western BOB in pentads 60–65 and the ICP in pentads 45–55. During pentads 45–55, the maximal precipitation is in the east sea of the Philippines along the ITCZ but that in the eastern SCS is earlier

in pentads 40–45. From southern China to the East China Sea and south of Japan, the maximal precipitation occurs in the spell of pentads 25–40 so the spot depicted in the previous studies (e.g., Zhang and Wang 2008; Qian and Tang 2010) disappeared. These pentads of maximal precipitation rate described here are same as that illustrated by Zhang and Wang (2008) from their six monsoon regions but we have shown all the pentads of maximal precipitation rate from the worldwide scope. If  $4 \text{ mm}\cdot\text{day}^{-1}$  precipitation rate is used as one of the thresholds, the duration of wet period at each place can be centered by the maximal precipitation pentad over the total consecutive pentads from Fig. 2a. In many regions such as in the equatorial eastern Africa, northern India, northern China, and from the Gulf of Mexico to the Caribbean Sea, the wet spell is from 2–10 pentads.

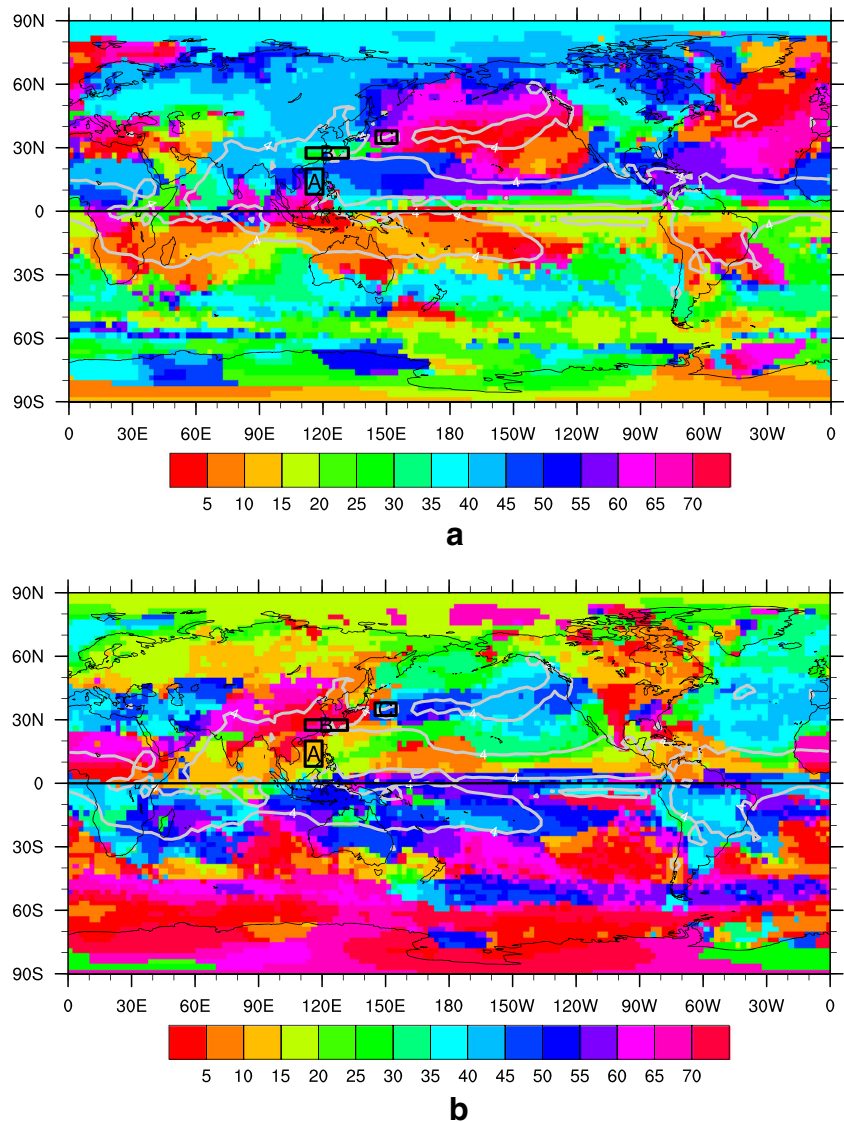
The pentad when precipitation rate reaches its minimum is also complicated as shown in Fig. 4b. But its progress is clear such as that from North China in pentads 60–70, central China in pentads 70–5, to the SCS in pentads 5–20. In SH, minimal precipitations appear in pentads 30–45 over the subtropical African and South American continents. A special region is located in the mid-North Pacific, where the precipitation difference is larger than  $4 \text{ mm}\cdot\text{day}^{-1}$  with the maximal precipitation in pentads 70–5 (winter) and the minimal precipitation in pentads 40–50 (autumn). It means that the maximal and minimal precipitation rates are not climatologically centered in the two pentads 8 and 44 as used by Qian and Tang (2010) or in the NH summer season (MJJAS) and the SH winter season (NDJFM) as used by Zhang and Wang (2008), even in the classical monsoon region. This phenomenon suggests that we cannot use a local pentad-mean or seasonal-mean dry-wet alteration as a threshold to identify if there is a monsoon region.

## 5 Dry-wet alteration and wind reversal

The cause of the dry-wet alteration and wind reversals is still debate question (Chao and Chen 2001; Ramage 1971; Webster 1987; Trenberth et al. 2000; Zeng and Li 2002). The wind and precipitation (or dry-wet) changes are closely and dynamically responses to solar seasonal radiation and sea-land thermal contrast. We here only identify the dry-wet alteration associated with wind reversal. In this analysis, there are several places with the difference between maximal and minimal precipitation rates exceeding  $4 \text{ mm}\cdot\text{day}^{-1}$  such as in the mid-North Pacific and the south of equatorial eastern Pacific, but it is not enough to indicate where the monsoon regions are. In previous studies, the tropical GM domain was identified, respectively, using dry-wet alteration (Qian et al. 1998a, 1998b; Qian 2000; Wang



**Fig. 4** Global distribution of pentads (five pentad interval) when precipitation rate climatologically reaches **a** maximum and **b** minimum, respectively. *Heavy white line* indicates the regions with the precipitation difference exceeding  $4 \text{ mm}\cdot\text{day}^{-1}$  as shown in Fig. 3e. Three boxes *A*, *B*, and *C* are, respectively, located in the eastern SCS ( $8\text{--}20^\circ \text{ N}$ ,  $112\text{--}120^\circ \text{ E}$ ), from South China to the East China Sea ( $25\text{--}30^\circ \text{ N}$ ,  $112\text{--}132^\circ \text{ E}$ ) and in the eastern part ( $32\text{--}38^\circ \text{ N}$ ,  $145\text{--}155^\circ \text{ E}$ ) of the western North Pacific monsoon domain

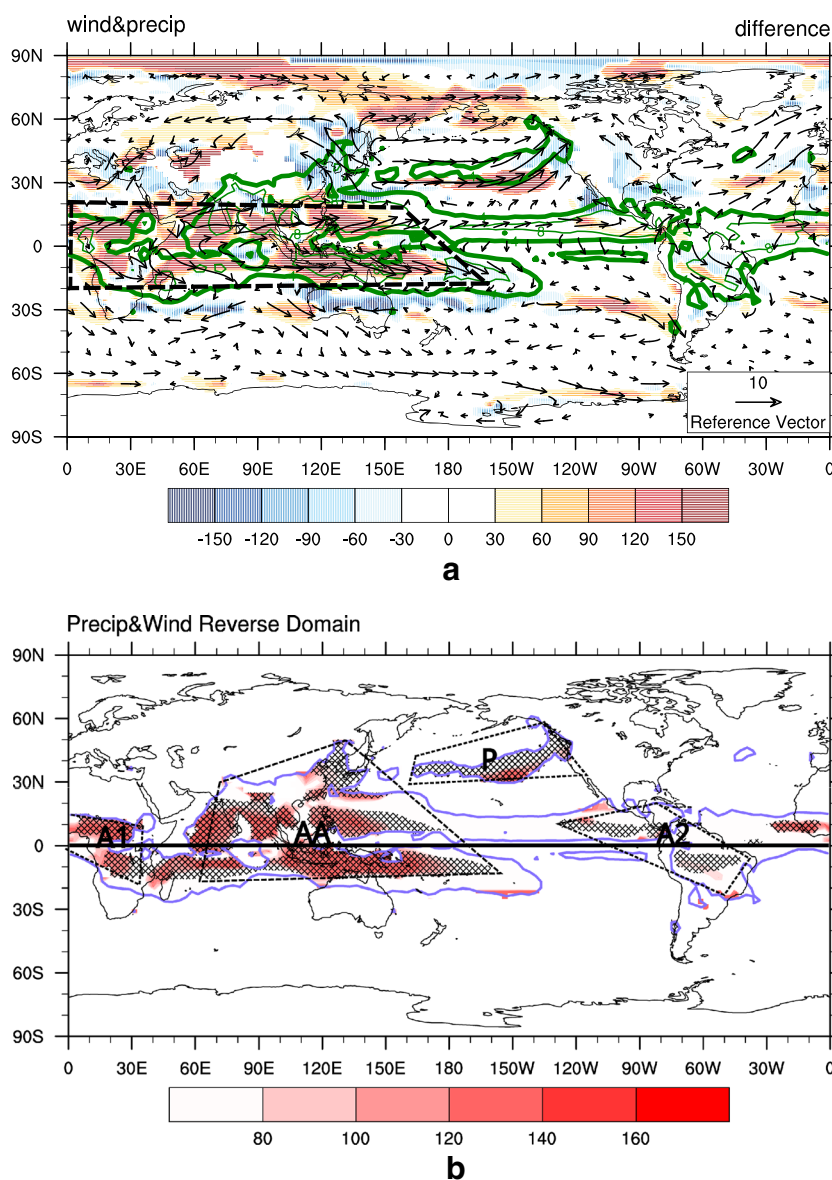


and Ding 2006) and wind reversal (Trenberth et al. 2000; Li and Zeng 2003) as well as a combination of the above two (Webster 1987; Qian et al. 2002a). To identify the tropical GM domain in detail, Fig. 5a shows the 850 hPa wind vector difference between the two pentads when precipitation rates reach the maximum and minimum, respectively. It is noted that prevailing wind reversal from both velocity and positive angle difference (clockwise) is predominantly located in the tropical Eastern Hemisphere (a heavy dashed area). This wind reversal region is entirely similar to that described by Khromov (1957) and Ramage (1971). Other significant regions of wind reversals are detected in the middle latitudes from East Asia to the NW Pacific as well as in the North Atlantic and the subtropical South America. Obviously, East Asia and the subtropical South America experience a negative angle change (anticlockwise). The reversal between southwesterly and northeasterly winds is

clearly observed in the north of the equatorial zone but with large velocity difference in the Eastern Hemisphere and small velocity difference in the eastern Pacific. Another reversal between northwesterly and southeasterly winds is observed in the south of the equatorial zone from Africa to Indian Ocean and western Pacific. The cross-equatorial flow can be noted in the East Africa, central Indian Ocean (south of Indian Peninsula), and from the maritime continents to the eastern Pacific. The changes from southwesterly to northwesterly winds is found over East Asia while that from northwesterly to easterly winds in the tropical South America (Qian et al. 2002a). In the mid-North Pacific, the reversal is caused by the interchange of westerly and easterly winds when the subtropical high center moves seasonally.

As an example for the SCS monsoon (Fig. 4 in the area A), its regional precipitation rate has at least three main

**Fig. 5** **a** Coverage exceeding  $4 \text{ mm}\cdot\text{day}^{-1}$  of global maximal and minimal pentad-mean precipitation rate differences (thick green line) and 850 hPa wind vector difference ( $\text{m}\cdot\text{s}^{-1}$ ) between the two pentads of the extrema of precipitation rates. Shadings are reversal angle ( $30^\circ$  interval) of the wind vector by the two pentads of maximal precipitation rate and minimal precipitation rate. Positive (negative) value indicates the wind vector reverses in clockwise (anti-clockwise) direction. **b** The thick dashed-line covers regions with the max-min precipitation rate difference exceeding  $4 \text{ mm}\cdot\text{day}^{-1}$ , red shading denotes alteration angle of wind direction between the two pentads larger than  $80^\circ$ , grey crossing lines denotes the wind difference exceeding  $5 \text{ m}\cdot\text{s}^{-1}$ . Letters “A1,” “AA,” “A2,” and “P” denote four regions of dry-wet alteration



maximum peaks (Qian and Yang 2000). The three peaks with the precipitation rate more than  $11 \text{ mm}\cdot\text{day}^{-1}$  are in late June, from July to August and in September while the minimum precipitation rate  $<2 \text{ mm}\cdot\text{day}^{-1}$  is in March and a rapid increase of precipitation rate from 2 to  $6 \text{ mm}\cdot\text{day}^{-1}$  occurs in middle May (Fig. 6a). The dry-wet difference for this rapid transition is  $4 \text{ mm}\cdot\text{day}^{-1}$ . The maximum precipitation rate using the first two harmonics peaks in late July while the peak in annual cycle is in early August. Other short-spell peaks are caused by the local small-scale climatic eddy turbulences. In the area B from South China to the East China Sea (Fig. 4) two major peaks of precipitation rate are in June (Fig. 6b). The combination (red line) is summed by the annual cycle (green line) and semiannual cycle (yellow line) and its peak is near the original pentad precipitation maximum (blue line). The summer (JJA or

MJJAS)-minus-winter (DJF or NDJFM) precipitation difference in the area A (SCS) is larger than  $4 \text{ mm}\cdot\text{day}^{-1}$  but this criterion cannot be used in the area B because the wet period is only about 1 month from late May to early June. The cross-equatorial flow (figure omitted) at 850 hPa in pentad 41 for the wet peak (Fig. 6a) has influenced the SCS. The cross-equatorial flow at 850 hPa for the wet peak (Fig. 6b) is approached from South China to south of Japan (Fig. 6c) and the wind reversal as well as the standardized pentad precipitation rate anomalies is clear from the SCS to South China and the East China Sea (Fig. 6d vs. Fig. 6c). In Fig. 6b, there are two large precipitation rate differences between climatology (blue line) and combined annual-semiannual cycles (red line) in pentads 34 and 39, respectively. Figures 6e, f, respectively, show the spatial differences of their precipitation rate and 850 hPa wind at the

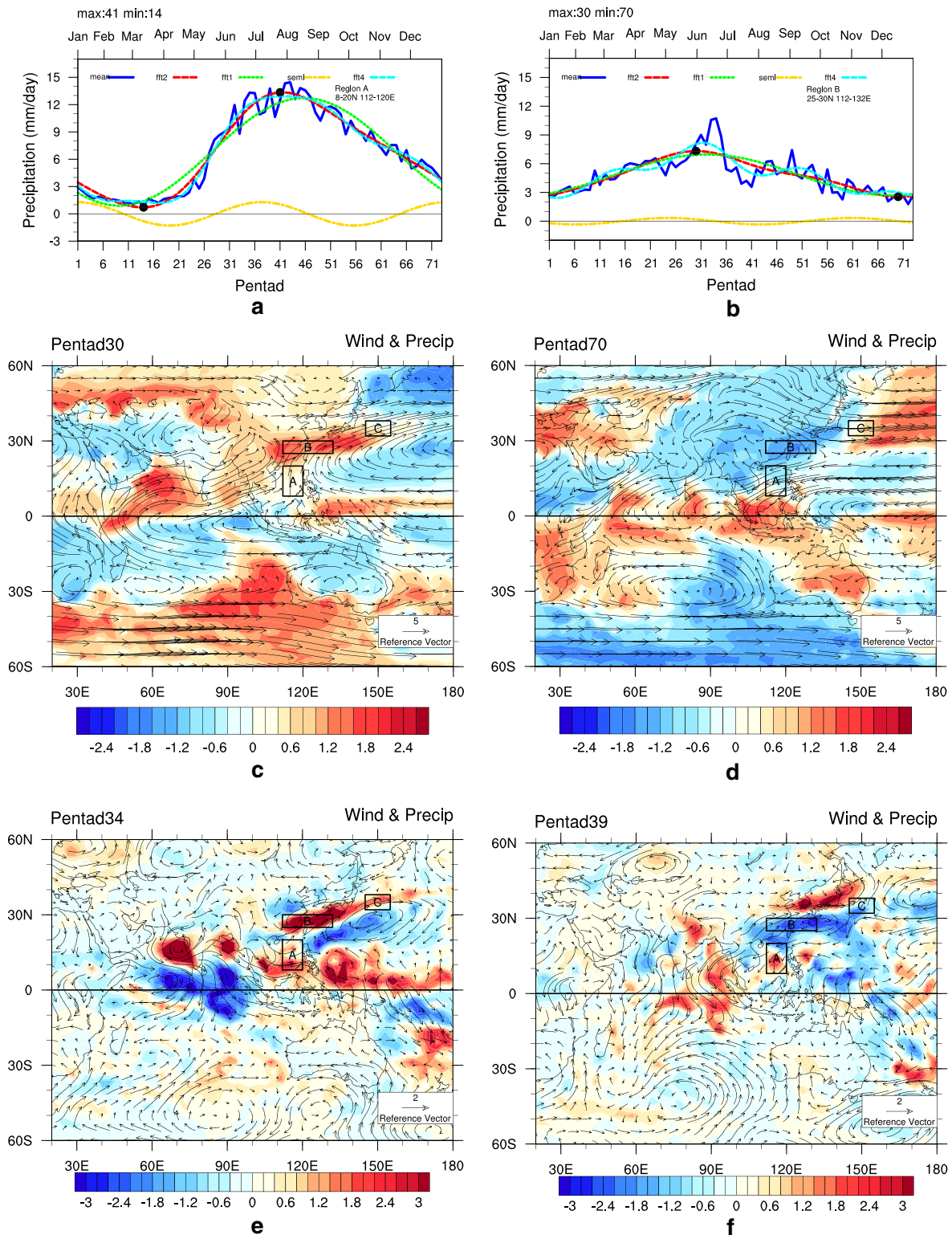


**Fig. 6** Pentad precipitation rates ( $\text{mm}\cdot\text{day}^{-1}$ ) in areas **a** A (SCS) and **b** B (South China and the East China Sea) as well as standardized pentad precipitation rate anomalies (standard deviation, SD) relative to the annual 73-pentad average and wind ( $\text{m}\cdot\text{s}^{-1}$ ) at 850 hPa in pentads **c** 30 and **d** 70. The differences of precipitation rate ( $\text{mm}\cdot\text{day}^{-1}$ ) and wind ( $\text{m}\cdot\text{s}^{-1}$ ) at pentads 34 and 39 based on original climatology and combined annual-semiannual cycles in Fig. 6b at pentads **e** 34 and **f** 39.

In **a** and **b**, original, annual cycle, semiannual cycle, and combined annual-semiannual cycle pentad precipitation rates as well as the first 4 harmonic components are indicated by blue, green, yellow, red, and cyan lines. Four heavy black dots in **a** and **b** along the red line denote their peaks at pentads 41 and 30 as well as valleys at pentads 14 and 70, respectively

two pentads. It is noted that the two differences of precipitation rate are caused by local climatic eddies (cyclone and anticyclone) from South China to south of Japan. It means that two opposite distributions of precipitation rate differences are not associated with the cross-equatorial flow at the lower troposphere. Although four harmonic components (cyan line in Fig 6b) approach the climatology but their spatial differences are caused by local climatic eddies (Figs. 6e, f).

Another example is the area C taken from the east sea of Japan (Fig. 4). In Fig. 7a, there are two major precipitation maximums in June and from October to November. The first maximum (red line) in early June is the monsoon precipitation because it is influenced by the cross-equatorial flow at 850 hPa as shown in Fig. 6c. The precipitation rate maximum in pentad 62 and minimum in pentad 45 as well

as their 850 hPa flow are shown in Figs. 7b, c. It is identified that the westerlies tend to locate to the west/northwest of the convective region. Thus, the wind reversal when the precipitation maximum is not clear in the region of wet-dry alternation in eastern part of the western North Pacific monsoon domain. In pentad 45 (Fig. 7c), the cross-equatorial flow can arrive to Northeast China but dry-wet transition beyond 50° N in Northeast Asia (Fig. 3) are influenced by the westerly flow at 850 hPa (Hu and Qian 2007).

Critical information from dry-wet alteration and prevailing wind reversal is extracted from Fig. 5a and presented in Fig. 5b. In this distribution, the mid-North Pacific and the south of equatorial eastern Pacific were excluded in the previous studies. According to the work of Wang and Ding (2008), the region in the mid-North Pacific belongs to the oceanic storm track. And, in our previous studies

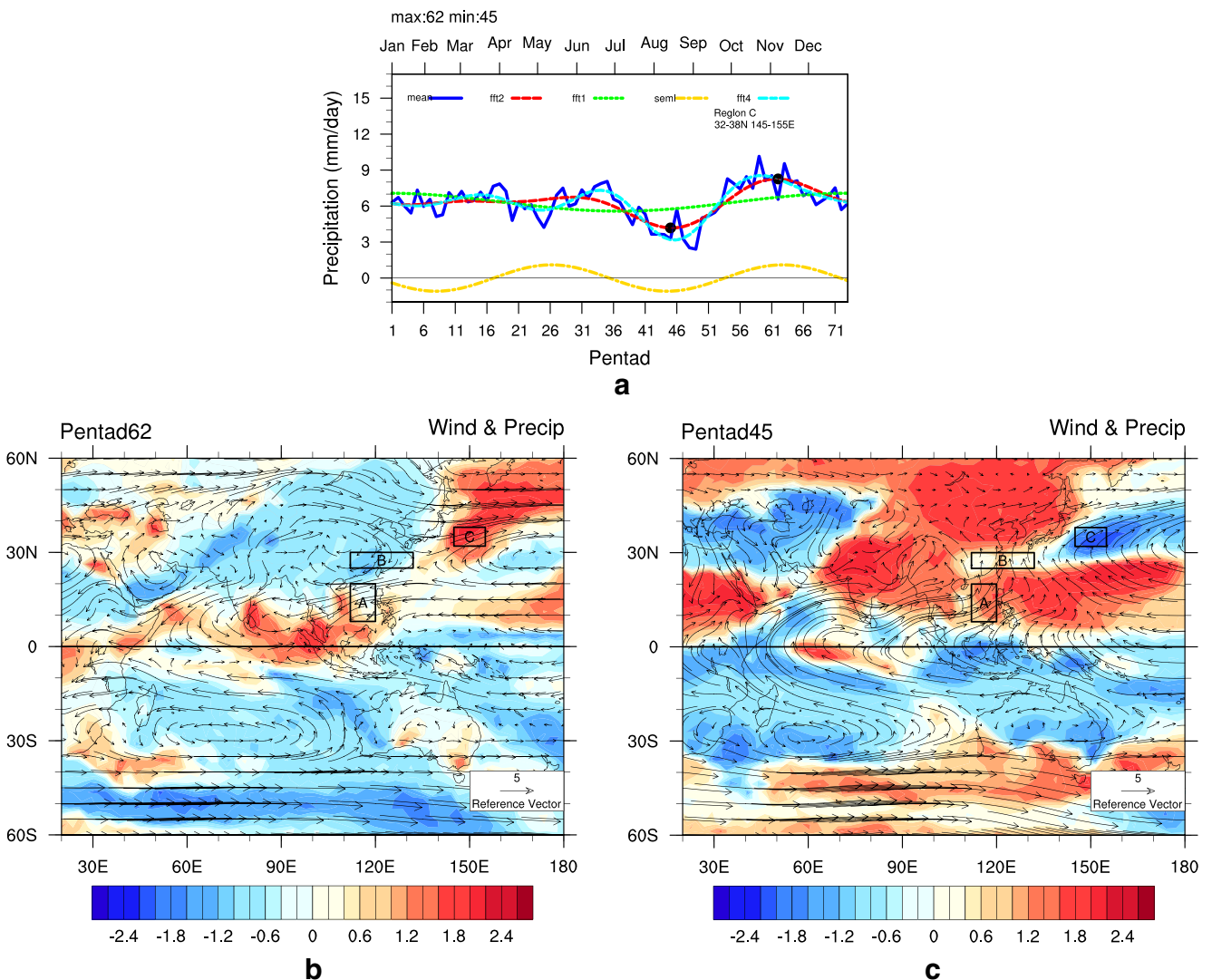


**Fig. 7** Same as in Fig. 6 except in the area “C” (eastern part of the western North Pacific monsoon domain) with two heavy black dots at pentads 62 and 45 in a. Two 850 hPa winds and standardized precipitation rates are at pentads 62 (c) and 45 (d)

(Qian and Yang 2000; Qian and Lee 2000; Qian 2000; Qian et al. 2002a), a monsoon region should be directly influenced by the low-level cross-equatorial flow. The dry-wet alternation in the mid-North Pacific is directly influenced by westerly flow and the subtropical anticyclone while that in the south of equatorial eastern Pacific by southeasterly flow. Therefore, the mid-North Pacific region is not counted as a monsoon region. After excluding the region in the mid-North Pacific, the tropical GM domain satisfying the dry-wet alteration and prevailing cross-equatorial wind reversal more than  $5 \text{ m}\cdot\text{s}^{-1}$  is clear in the tropical South and North Africa, from South Asia to East Asia and the tropical NW Pacific, and from the subtropical Indian Ocean to the maritime continents. It is noted that if only considering dry-wet alteration, other two regions in the north of equatorial central-eastern Pacific along the Pacific ITCZ and from the tropical South America to the tropical Atlantic, are also included in the tropical GM domain.

From the above description, four regions with dry-wet alteration marked by A1, AA, A2, and P in Fig. 5b can be categorized into two classical monsoon regions and a non-classical monsoon region as well as a non-monsoon region, respectively. Region A1 located in the tropical Africa and region AA situated between Asia and Australia are influenced by the cross-equatorial flow with the wind reversal larger than  $120^\circ$  or wind velocity difference exceeding  $5 \text{ m}\cdot\text{s}^{-1}$ . These two regions are consistent with the description of Khromov (1957) and Ramage (1971) so they are referred as the classical global monsoon domain. Region A2 located in the tropical America is influenced by the cross-equatorial flow with the wind difference exceeding  $5 \text{ m}\cdot\text{s}^{-1}$  but the wind reversal is smaller than  $120^\circ$ . This region is not considered by the description of Khromov (1957) and Ramage (1971) so it is referred as the non-classical monsoon region. Region P located in the mid-North Pacific is not influenced by the cross-equatorial flow, although its wind difference is more than  $5 \text{ m}\cdot\text{s}^{-1}$  and the wind reversal is larger than  $120^\circ$  so it is referred as the non-monsoon region. The wind reversal in early November when the precipitation maximum is not clear in the region of wet-dry alternation in eastern part of the western North Pacific monsoon domain but its second precipitation maximum in June

is influenced by the cross-equatorial flow at 850 hPa. The categories and features from this classification are given in Table 1. The region P is caused by the polar front when its location is seasonally shifted. Similar location shift of polar frontal precipitation can also be observed in the middle latitudes over the North Atlantic and SH (dotted line in Fig. 3).

Some basic climatic features of the tropical monsoon dry-wet alteration and prevailing wind change can be further identified from Fig. 8. Figure 8a shows the latitude-pentad section of pentad-mean precipitation rate, 850 hPa wind vectors and 850 hPa temperature averaged from the whole latitude circle by the following algorithm

$$[\tilde{F}_d(\varphi, p)] = \sum_{\lambda=1}^I \tilde{F}_d(\lambda, \varphi, p) \tag{3}$$

where  $I = 144$ ,  $p = 850 \text{ hPa}$ . An average dry-wet alteration can be identified in Fig. 8a by  $6 \text{ mm}\cdot\text{day}^{-1}$  precipitation rate with an asymmetric wet spell in the NH from pentads 18 to 71. The southernmost and northernmost locations of  $6 \text{ mm}\cdot\text{day}^{-1}$  line and easterly flow (trade, black dashed line) in the two hemispheres appear in pentads 8 and 44. In each hemisphere, wet spell appears during the period of weak trade and poleward wind.

In meteorological community, the study of South Asian monsoon has a long history. Figure 8b shows the latitude-pentad section of the three climatic variables averaged from longitudes between  $60^\circ \text{ E}$  and  $100^\circ \text{ E}$ . A reversal of easterly and westerly wind directions features in pentads 24 and 56. The precipitation rate reaches a high flat from pentads 30 to 56. The strongest southwesterly flow peaks in pentad 44 but the temperature peaks in pentad 53.

A unique feature can be identified for the SCS summer monsoon. In previous studies, an abrupt onset of the summer monsoon observed from dry-wet alteration and easterly-westerly wind reversal is from pentads 27 to 28 (middle of May) in the central SCS (Qian and Yang 2000; Qian and Lee 2000). This feature is also clearly indicated by the  $4 \text{ mm}\cdot\text{day}^{-1}$  (or  $6 \text{ mm}\cdot\text{day}^{-1}$ ) precipitation line and wind direction turning from easterly to southwesterly flow

**Table 1** Categories and features of global dry-wet alteration regions. Four regions marked by A1, AA, A2, and P are shown in Fig. 5b

Category	Region	Wind angle change > 120 degrees	Wind difference > $5 \text{ m}\cdot\text{s}^{-1}$	Crossequatorial flow influence
Classical monsoon	African monsoon (A1)	Yes	Yes	Yes
	Asian-Australian Monsoon (AA)	Yes	Yes	Yes
Non-classical monsoon	American Monsoon (A2)	No	Yes	Yes
Nonmonsoon	Mid-North Pacific (P)	Yes	Yes	No

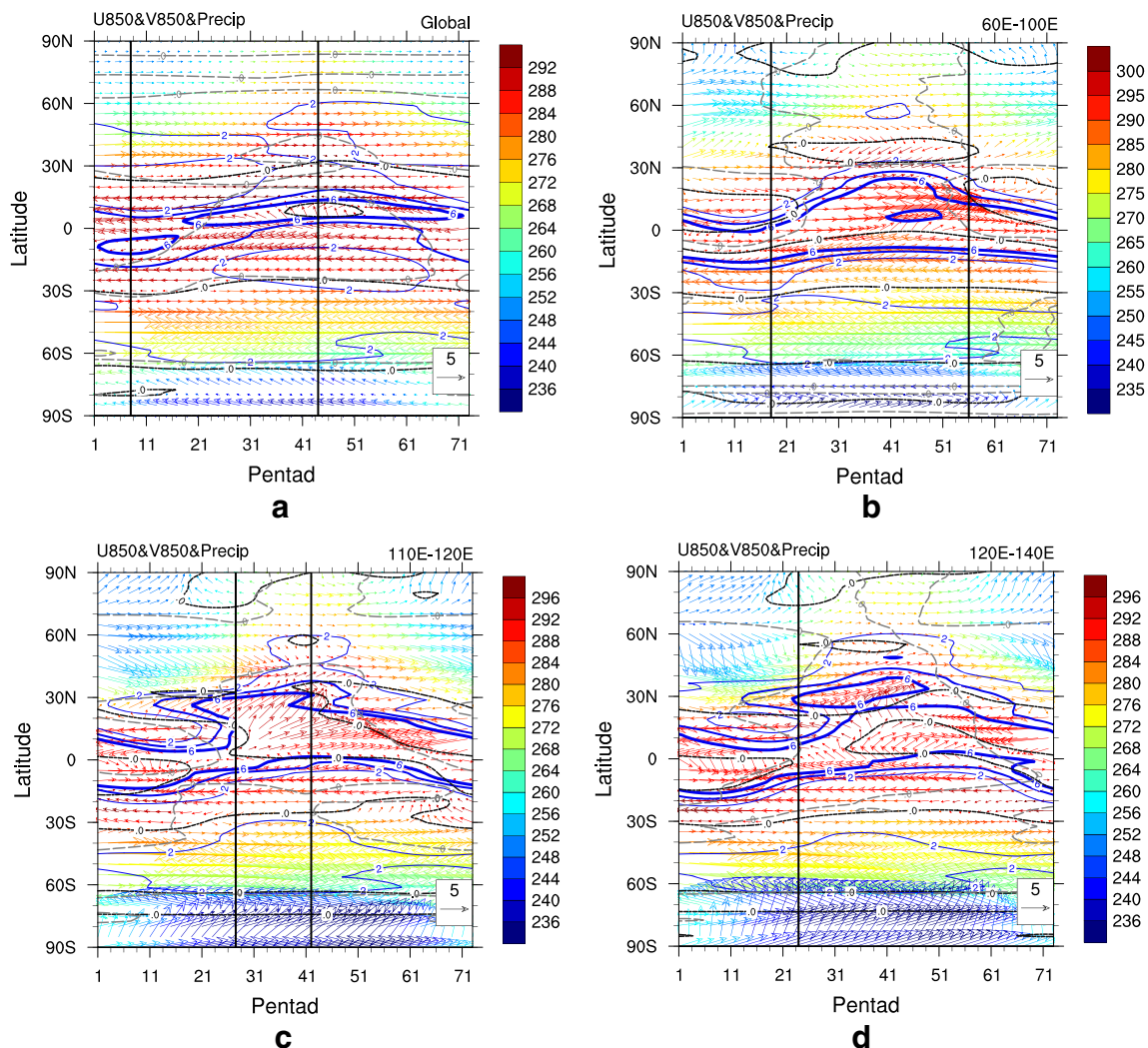


**Fig. 8** Latitude-pentad sections of climatological pentad-mean precipitation (*solid blue line*,  $2 \text{ mm}\cdot\text{day}^{-1}$  interval), 850 hPa wind vectors ( $\text{m}\cdot\text{s}^{-1}$ ) and 850 hPa temperature (*shading*,  $4 \text{ K}$  interval) averaged from **a** the whole latitude circle, **b**  $60\text{--}100^\circ \text{ E}$ , **c**  $110\text{--}120^\circ \text{ E}$ , and

**d**  $120\text{--}140^\circ \text{ E}$  longitudes widths, respectively. *Heavy straight lines* are marked in pentads **a** 8 & 44, **b** 18 & 56, **c** 27–28 & 42, and **d** 24. The *thin black (grey) dashed line* indicates the zero line of zonal (meridional) wind

(Fig. 8c). Between  $20$  and  $30^\circ \text{ N}$  over southern China, the southwesterly flow is gradually increased from pentads 1 to 46 but the  $6 \text{ mm}\cdot\text{day}^{-1}$  precipitation line starts from pentads 20 to 42. Only after the onset of central SCS monsoon, southwesterly flow and  $2 \text{ mm}\cdot\text{day}^{-1}$  precipitation line extend northward from the Yangtze River to the Yellow River. Beyond the latitude of  $45^\circ \text{ N}$ , the  $2 \text{ mm}\cdot\text{day}^{-1}$  precipitation rate corresponds with the northwesterly flow so summer monsoon precipitation should be regarded as a condition of poleward moisture transport influenced by the cross-equatorial flow.

The western Pacific monsoon is also a well-studied topic (e.g., Tanaka 1992; Holland 1995; Ueda and Yasunari 1995; Wang and Lin 2002). Figure 8d shows the latitude-pentad cross section of the three climatic variables averaged over

the longitudes between  $120^\circ \text{ E}$  and  $140^\circ \text{ E}$ . There are two regions covered by the  $6 \text{ mm}\cdot\text{day}^{-1}$  precipitation line, which are separated in the subtropical NW Pacific from pentads 24 to 48. Near  $30^\circ \text{ N}$ , the southwesterly flow and  $6 \text{ mm}\cdot\text{day}^{-1}$  line are similar to that shown in Fig. 8c. Between  $40\text{--}50^\circ \text{ N}$ , the transition from a cold northwesterly flow to a warm southwesterly flow start from the central SCS monsoon onset. In this width of longitudes, the southwesterly flow can reach  $50^\circ \text{ N}$  and the precipitation falls over Japanese islands and the Korean Peninsula (Qian et al. 2002b).

Several important pentads are highlighted in Fig. 8. Thus, their spatial structures of pentad-mean precipitation rate and warm-cold flows at 850 hPa are also illustrated in this section. Figure 9a shows these structures in pentad 8. An

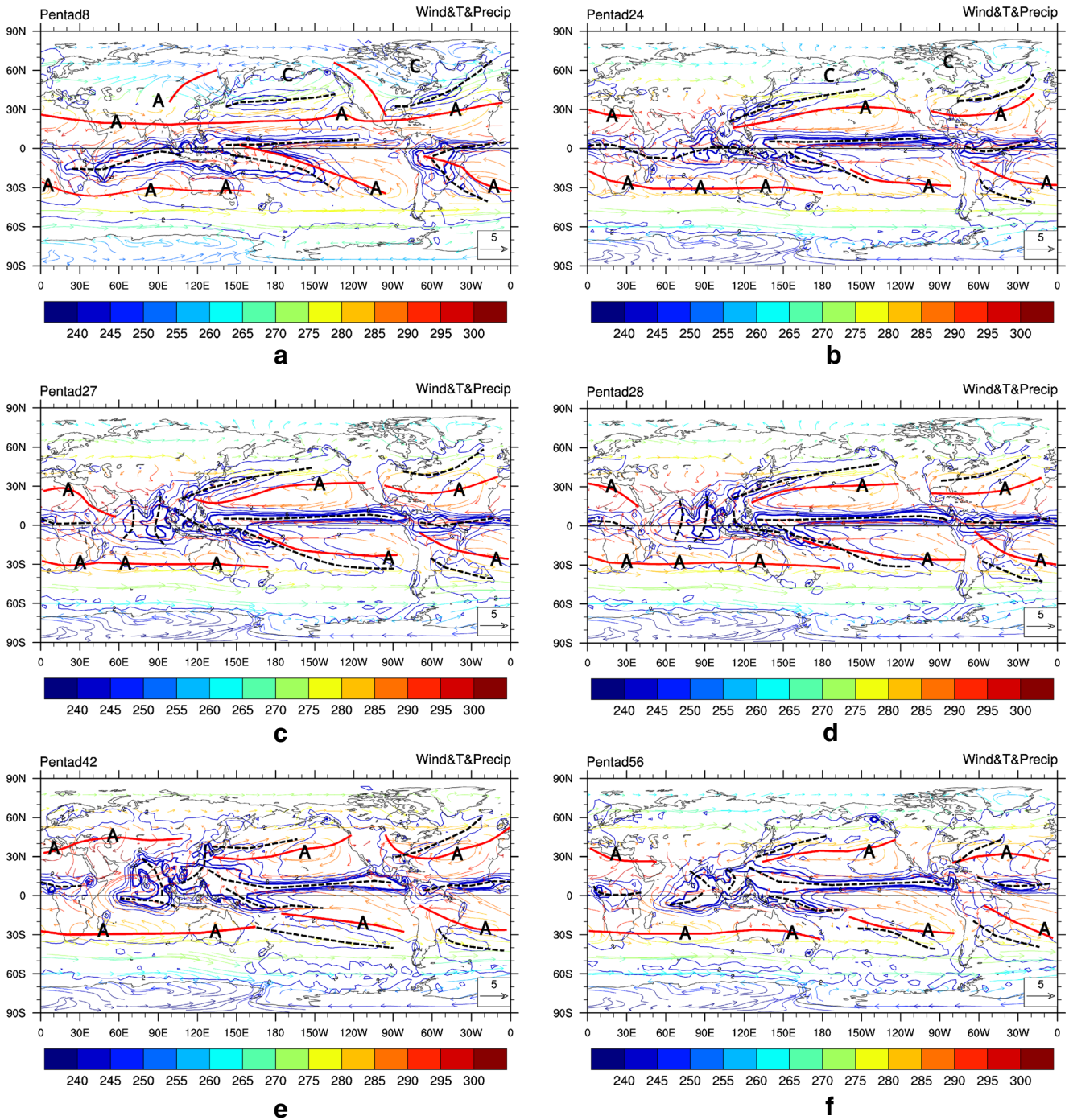


**Fig. 9** Climatic precipitation rate (*solid blue line*,  $2 \text{ mm-day}^{-1}$  interval) and climatic wind at 850 hPa (*arrow*,  $\text{m-s}^{-1}$ ) and climatic temperature (*shading*, 5 K interval) in **a** pentad 8, **b** pentad 24, **c** pentad 27, **d** pentad 28, **e** pentad 42, and **f** pentad 56. The

*thick red line* denotes subtropical high (anticyclone) ridge while the *thick black-dashed line* is along the axis of precipitation rate. Letters "A" and "C" denote the locations of anticyclone and cyclone, respectively

axis of precipitation rate in the south of equator from subtropical Africa to the Southwest Pacific is ended at the northerly flow. It implies that the axis of precipitation rate is also the convergence line in the austral summer. The wind direction changes when it crosses the convergence

line. Another axis of precipitation rate in the north of equatorial North Pacific accompanies by a convergence between southeasterly and northeasterly flows. Thus, the two convergence zones in the tropical western Pacific are resulted from different flows. The former is termed monsoon

convergence zone while the latter is trade wind convergence zone. In the tropical Atlantic, two axes of precipitation rate are accompanied well by a monsoon convergence zone and a trade convergence zone. These axes of precipitation rate in the tropics are low-pressure zones and flow convergence zones, separated by the subtropical high circulation systems. In the mid-North Pacific and mid-North Atlantic, there are two axes of precipitation rate, which are along the storm tracks and resulted from polar frontal activity seasonally in the boreal winter.

Pentad 24 is a transition time from the boreal winter half to the summer half of a year so tropical flow convergence zone and precipitation rate axis are mostly approached to the equator. At this time, the cross-equatorial flow is very weak (Fig. 9b). All subtropical anticyclone systems in SH move equatorward while anticyclone systems in NH are enhanced and move westward relative to that in pentad 8. Meanwhile, two axes of frontal precipitation in NW Pacific and NW Atlantic extend westward to southern China and eastern America, respectively.

In pentad 27, an obvious feature is that the central SCS is still dry (not covered by 6 or 4 mm·day<sup>-1</sup> line) and the subtropical NW Pacific high ridge is also controlled in the central SCS (Fig. 9c). At this time, 6 mm·day<sup>-1</sup> line covers the eastern Arabian Sea, the BOB and the southern part of SCS, influenced by southwesterly cross-equatorial flow. Meanwhile, 6 mm·day<sup>-1</sup> line has covered over southern China while the axis of precipitation rate is a frontal place extending westward. Actually, the westerly flow is still prevailing over the Indian Peninsula, the ICP and southern China (Figs. 9a–c). Therefore, the precipitation in southern China is not influenced by the cross-equatorial monsoon flow at the moment. An abrupt dry-wet alteration occurs in the central SCS by the 6 mm·day<sup>-1</sup> line in pentad 28 (Fig. 9d). Surrounding the neighboring seas of Asian continent, 6 mm·day<sup>-1</sup> line and cross-equatorial southwesterly flow arrive at the Arabian Sea, the BOB, the SCS, and southern China because the subtropical high ridge has withdrawn from the SCS. Actually, these basic features of the SCS summer monsoon onset have been revealed a decade ago using different dataset (Qian and Yang 2000; Qian and Lee 2000).

In pentad 42, two subtropical highs in North Pacific and North Atlantic have reached the strongest stage and the northernmost location so the Asian summer monsoon flow also reaches its strongest stage and the northernmost location, particularly in Northeast Asia (Fig. 9e). In this pentad, the trade wind convergence zone (or ITCZ) has also reached the strongest in the equatorial Pacific and the equatorial Atlantic. Another alteration time from the boreal summer to the winter half year is in pentad 56 (Fig. 9f) but the tropical precipitation is stronger than the former seasonal alteration in pentad 24 because the 6 mm·day<sup>-1</sup> line still covers the

SCS, although the 4 mm·day<sup>-1</sup> line has left southern China. The axis of precipitation rate over the tropical Southwest Pacific is now located in the trough between the two anticyclones centered in Australia and the subtropical Southeast Pacific.

Globally and seasonally, the distribution of pentad-mean precipitation rate corresponds well with major large-scale circulation systems forced by seasonal solar radiation and sea-land contrasts as illustrated in Fig. 9. In NH Pacific, the longest zonally oriented axis of pentad-mean precipitation rate in the north of the equatorial Pacific is caused by the ITCZ. Another axis of pentad-mean precipitation rate in mid-latitudes is the storm track location associated with the interaction between the westerly flow and the subtropical North Pacific high circulation with its high center moving southwestward from spring to summer. Two precipitation rate axes in the NH Atlantic along the ITCZ and the storm track are similar to that in the NH Pacific. In the SH, two precipitation rate axes in the tropical Southwest Pacific and in the tropical Southwest Atlantic are caused by the interactions between two adjacent anticyclones and middle-latitude westerly flow. In the tropical Indian Ocean, a zonally oriented precipitation rate axis is along the austral summer ITCZ. Between Asia and Australia as well as over the tropical African continents, the distribution of pentad-mean precipitation rate is complicated. The precipitation rate axis in the south of equatorial Africa is formed in the boreal summer and caused by the interaction of northeasterly flow from South Asia with two adjacent subtropical anticyclones in the Indian and Atlantic oceans. Another precipitation rate axis in the north of equatorial Africa is connected with the ITCZ in the equatorial Atlantic. Several centers of pentad-mean precipitation rate situated in the neighboring seas of Asian continent are associated with peninsular-scale monsoon troughs (Qian and Tang 2010). The difference exceeding 4 mm·day<sup>-1</sup> between maximal and minimal pentad-mean precipitation rates captures the global dry-wet alteration. Although some spots such as from southern China to the East China Sea cannot be found from this difference, there are some places with large precipitation difference in mid-latitudes such as in the mid-North Pacific and the mid-North Atlantic.

## 6 Summary and discussion

How to identify and understand monsoon has been discussed for about half a century. The early monsoon description was based on the frequency of prevailing wind from the global scale. Since the late 1970s, satellites have been providing worldwide observation. Thus, the global-scale dry-wet or convective description became climatologically



possible in the 1990s. Therefore, the term of global monsoon was naturally proposed and used in literature. Meanwhile, many indices have also been proposed to picture the global monsoon. However, abrupt dry-wet seasonal alteration can be found from two adjacent regions or consecutive months even pentads, thus some questions concerning the global monsoon domain still remain.

A new index based on the climatic difference between maximal and minimal precipitation rates exceeding  $4 \text{ mm}\cdot\text{day}^{-1}$  from two calendar pentads was used to identify the regions of dry-wet alteration. Along the equatorial zone, there is a large portion without experiencing seasonal dry-wet alteration. Thus, dry-wet alteration is mainly concentrated in two subtropical zones. From South Asia to the subtropical NW Pacific, the region of dry-wet alteration is wider than other subtropical regions in the NH. In East Asia, dry-wet alteration has even extended to Northeast China and the Korean Peninsula near  $45^\circ \text{ N}$ , but almost no dry-wet alteration in the Arabian region. There is a very narrow zone of dry-wet alteration in the south of equatorial eastern Pacific and another dry-wet alteration in the middle latitude of North Pacific.

The timing of the seasonal dry-wet alteration can be identified in more detail at various locations. The most complicated is observed in Asia but much simpler over ocean. Pentads of maximal precipitation rate are 30–40 in the Arabian Sea, 40–45 in the Indian Peninsula, 60–65 in the western BOB, 35–40 in the eastern BOB, 45–55 in the Indo-China Peninsular, 40–45 in the central SCS, and 28–35 from southern China to Japan. In mid-latitudes of North Pacific, maximal precipitation rate mainly appears in the boreal winter from pentads 60–73–10. In the subtropical SH, maximal precipitation rate appears from pentads 1–25.

Finally, cause behind the dry-wet alteration was explored mainly from low-level wind changes or atmospheric circulation systems. Two dry-wet alteration regions in the north of equatorial eastern Pacific and the north of equatorial Atlantic are linked with two hemispheric subtropical anticyclones and associated with the shift of ITCZ locations with little wind direction change. In the south of equatorial eastern Pacific, there is a small dry-wet alteration region but without experiencing wind direction change. In the mid-latitude of North Pacific, there is a dry-wet alteration region together with prevailing wind reversal but its wind is not coming from the low-level cross-equatorial flow. The global monsoon domain satisfying dry-wet alteration and prevailing wind reversal associated with the low-level cross-equatorial flow is mainly located in the tropical Eastern Hemisphere from the tropical Africa to tropical western Pacific including South Asia, East Asia, tropical NW Pacific, and the maritime continents.

After the analysis about where experiences and what causes the dry-wet alteration, some regional differences of calendar maximal and minimal precipitation rates in two pentads can be well explained. In the subtropical SH, there should be only a circular zone of dry-wet alteration if not considering the sea-land distributions, so persistent dry regions in the subtropical Southeastern Pacific and the subtropical South Atlantic are influenced by the three continents. The breadth of dry-wet alteration regions from South Asia to East Asia and the subtropical NW Pacific, and the absence of dry-wet alteration in the Arabian region are influenced by the Tibetan Plateau and forced by the contrast between the Asian continent and the Indian Ocean.

The global main regions of dry-wet alteration are distinguished by whether it is influenced by the low-level cross-equatorial flow with wind difference exceeding  $5 \text{ m}\cdot\text{s}^{-1}$  and wind angle change larger than  $120^\circ$ . The classical monsoon domain satisfying this condition is confirmed from the tropical Africa and tropical Asia-Australia region. The non-classical monsoon region satisfying the low-level cross-equatorial flow with the wind difference exceeding  $5 \text{ m}\cdot\text{s}^{-1}$  but wind angle change smaller than  $120^\circ$  is located in the tropical America. The non-monsoon region satisfying the wind difference exceeding  $5 \text{ m}\cdot\text{s}^{-1}$  and wind angle change larger than  $120^\circ$  but with no influence of the low-level cross-equatorial flow found in the mid-North Pacific.

Since the late 1990s, different definitions were used to identify the global monsoon domain. Even in the global monsoon domain identified in this paper, the appearance time of maximal pentad-mean precipitation rate is complicated. Therefore, how many monsoon regions can be objectively divided from the global monsoon domain is another question which will be studied in the subsequent part.

## References

- Adams DK, Comrie AC (1997) The North American monsoon. *Bull Am Meteorol Soc* 78(10):2197–221
- Barlow M, Cullen H, Lyon B (2002) Drought in central and southwest Asia: La Niña, the warm pool, and Indian Ocean precipitation. *J Clim* 15(7):697–700
- Chao WC, Chen B (2001) The origin of monsoons. *J Atmos Sci* 58(22):3497–3507
- Chen L, Zhu Q, Luo H, He J, Dong M, Feng Z (1991) The East Asian Monsoon. Beijing Meteorological Press, Beijing (In Chinese)
- Chu JL, Kang H, Tam CY, Park CK, Chen CT (2008) Seasonal forecast for local precipitation over northern Taiwan using statistical downscaling. *J Geophys Res: Atmos* 113(D12):1984–2012
- Holland G (1995) Scale interaction in the western Pacific monsoon. *Meteorol Atmos Phys* 56(1–2):57–79

- Hu H, Qian W (2007) Identifying the northernmost summer monsoon location in East Asia. *Prog Nat Sci* 17(7):812–820
- Khromov SP (1957) Die geographische verbreitung der monsune. *Petermanns Geogr Mitt* 101:234–237
- Kim HJ, Wang B, Ding Q (2008) The global monsoon variability simulated by CMIP3 coupled climate models. *J Clim* 21(20):5271–5294
- Lau K, Yang S (1997) Climatology and interannual variability of the Southeast Asian summer monsoon. *Adv Atmos Sci* 14(2):141–162
- Li J, Zeng Q (2002) A unified monsoon index. *Geophys Res Lett* 29(8):115–1
- Li J, Zeng Q (2003) A new monsoon index and the geographical distribution of the global monsoons. *Adv Atmos Sci* 20(2):299–302
- Liu J, Wang B, Ding Q, Kuang X, Soon W, Zorita E (2009) Centennial variations of the global monsoon precipitation in the last millennium: results from ECHO-G model. *J Clim* 22(9):2356–2371
- Liu Z, Harrison S, Kutzbach J, Otto-Bliessner B (2004) Global monsoons in the mid-Holocene and oceanic feedback. *Clim Dyn* 22(2-3):157–182
- Masao K, Wesley E, Jack W, Yang SK, JJ H, Fiorino M, Potter G (2002) NCEP/DOE AMIP-II Reanalysis (R-2). *Bull Am Meteorol Soc* 83(11):1631–1643
- McBride JL (1987) The Australian summer monsoon. In: Chang CP, Krishnamurty T (eds) *Monsoon Meteorology*. Oxford University Press, pp 203–231
- Nguyen DQ, Renwick J, McGregor J (2014) Variations of monsoon rainfall: a simple unified index. *Geophys Res Lett* 41(2):575–581
- Nicholson SE, Kim J (1997) The relationship of the El Niño–Southern Oscillation to African rainfall. *Int J Climatol* 17(2):117–135
- Qian W (2000) Dry/wet alternation and global monsoon. *Geophys Res Lett* 27(22):3679–3682
- Qian W, Jiang M (2014) Early signals of synoptic-scale atmospheric anomalies associated with the summer low temperature events in Northeast China. *Meteorol Atmos Phys* 124(1-2):33–46
- Qian W, Lee DK (2000) Seasonal march of Asian summer monsoon. *Int J Climatol* 20(11):1371–1386
- Qian W, Tang S (2010) Identifying global monsoon troughs and global atmospheric centers of action on a pentad scale. *Atmospheric and Oceanic Science Letters* 3(1):1–6
- Qian W, Yang S (2000) Onset of the regional monsoon over Southeast Asia. *Meteorol Atmos Phys* 75(1-2):29–38
- Qian W, Zhu Y (2002) The comparison between summer monsoon components over East Asia and South Asia. *J Geosciences of China* 4(3-4):17–32
- Qian W, Ye Q, Zhu Y (1998a) Monsoonal oscillation revealed by the upper-troposphere water vapor band brightness temperature. *Chinese Science Bulletin* 43(17):1489–1494
- Qian W, Zhu Y, Xie A, Ye Q (1998b) Seasonal and interannual variations of upper tropospheric water vapor band brightness temperature over the global monsoon regions. *Adv Atmos Sci* 15:337–345
- Qian W, Deng Y, Zhu Y, Dong W (2002a) Demarcating the worldwide monsoon. *Theor Appl Climatol* 71(1-2):1–16
- Qian W, Kang HS, Lee DK (2002b) Distribution of seasonal rainfall in the East Asian monsoon region. *Theor Appl Climatol* 73(3-4):151–168
- Qian W, Lin X, Zhu Y, Xu Y, Fu J (2007) Climatic regime shift and decadal anomalous events in China. *Clim Chang* 84(2):167–189
- Qian W, Ding T, Hu H, Lin X, Qin A (2009) An overview of dry-wet climate variability among monsoon-westerly regions and the monsoon northernmost marginal active zone in China. *Adv Atmos Sci* 26:630–641
- Qian W, Chen Y, Jiang M, Hu Q (2015) An anomaly-based method for identifying signals of spring and autumn low temperature events in the Yangtze River Valley, China. *J Appl Meteorol Climatol* (in press)
- Ramage CS (1971) *Monsoon meteorology* (vol. 15 of international geophysics series). Academic Press
- Sankar-Rao M (1966) Equations for global monsoons and toroidal circulations in the  $\sigma$ -coordinate system. *Pure and Applied Geophysics* 65(1):196–215
- Sankar-Rao M, Saltzman B (1969) On a steady state theory of global monsoons. *Tellus* 21(3):308–330
- Song F, Zhou T, Qian Y (2014) Responses of East Asian summer monsoon to natural and anthropogenic forcings in the 17 latest CMIP5 models. *Geophys Res Lett* 41(2):596–603
- Sperber KR, Annamalai H, Kang IS, Kitoh A, Moise A, Turner A, Wang B, Zhou T (2013) The Asian summer monsoon: an inter-comparison of CMIP5 vs. CMIP3 simulations of the late 20th century. *Clim Dyn* 41(9-10):2711–2744
- Tanaka M (1992) Intraseasonal oscillation and the onset and retreat dates of the summer monsoon over east, southeast Asia and the western Pacific region using GMS high cloud amount data. *J Meteorol Soc Jpn* 70(1B):613–629
- Tang S, Qian W (2009) Asian-Australian monsoon troughs and monsoon precipitation influenced by regional land-sea heating contrasts. *J Trop Meteorol*:S1
- Tao S, Chen L (1987) A review of recent research on the East Asian summer monsoon in China. In: *Monsoon Meteorology*. Oxford University Press
- Tippett MK, Goddard L, Barnston AG (2005) Statistical-dynamical seasonal forecasts of central-southwest Asian winter precipitation. *J Clim* 18(11):1831–1843
- Trenberth KE, Stepaniak DP, Caron JM (2000) The global monsoon as seen through the divergent atmospheric circulation. *J Clim* 13(22):3969–3993
- Ueda H, Yasunari T, Kawamura R (1995) Abrupt seasonal change of large-scale convective activity over the western Pacific. *J Meteorol Soc Jpn* 73(4):795–809
- Wang B (1994) Climatic regimes of tropical convection and rainfall. *J Clim* 7(7):1109–1118
- Wang B, Ding Q (2006) Changes in global monsoon precipitation over the past 56 years. doi:10.1029/2005GL025347
- Wang B, Ding Q (2008) Global monsoon: dominant mode of annual variation in the tropics. *Dyn Atmos Oceans* 44(3):165–183
- Wang B, Fan Z (1999) Choice of South Asian summer monsoon indices. *Bull Am Meteorol Soc* 80(4):629–638
- Wang B, Lin H (2002) Rainy season of the Asian-Pacific summer monsoon. *J Clim* 15(4):386–398
- Wang B, Wu Z, Li J, Liu J, Chang CP, Ding Y, Wu G (2008) How to measure the strength of the East Asian summer monsoon. *J Clim* 21(17):4449–4463
- Wang B, Liu J, Kim HJ, Webster PJ, Yim SY (2012) Recent change of the global monsoon precipitation (1979–2008). *Clim Dyn* 39(5):1123–1135
- Wang P (2009) Global monsoon in a geological perspective. *Chin Sci Bull* 54(7):1113–1136
- Wang P, Wang B, Kiefer T (2009) Global monsoon in observations, simulations and geological records. *PAGES News* 17(2):82–83
- Wang P, Wang B, Cheng H, Fasullo J, Guo Z, Kiefer T, Liu Z (2014) The global monsoon across time scales: is there coherent variability of regional monsoons? *Clim Past Discuss* 10:2163–2291
- Webster PJ (1981) Monsoons. *Sci Am* 245:108–118
- Webster PJ (1987) The elementary monsoon. In: Fein JS, Stephens PL (eds). *Monsoons* John Wiley, pp 3–32
- Webster PJ, Magana VO, Palmer T, Shukla J, Tomas R, Yanai Mu, Yasunari T (1998) Monsoons: Processes, predictability, and the

- prospects for prediction. *J Geophys Res: Oceans* (1978–2012) 103(C7):14 510:451–14
- Xie P, Arkin PA (1997) Global precipitation: a 17-year monthly analysis based on gauge observations, satellite estimates, and numerical model outputs. *Bull Am Meteorol Soc* 78(11):2539–2558
- Zeng Q, Li J (2002) Interactions between the Northern and Southern Hemispheric atmospheres and the essence of monsoon. *Chinese J Atmos Sci* 26(4):433–448
- Zeng X, Lu E (2004) Globally unified monsoon onset and retreat indexes. *J Clim* 17(11):2241–2248
- Zhang S, Wang B (2008) Global summer monsoon rainy seasons. *Int J Climatol* 28(12):1563–1578
- Zhao P, Jiang P, Zhou X, Zhu C (2009) Modeling impacts of East Asian ocean-land thermal contrast on spring southwesterly winds and rainfall in eastern China. *Chin Sci Bull* 54(24):4733–4741
- Zhou J, Lau K (1998) Does a monsoon climate exist over South America? *J Clim* 11(5):1020–1040
- Zhu C, Zhou X, Zhao P, Chen L, He J (2011) Onset of East Asian subtropical summer monsoon and rainy season in China. *Sci China Earth Sci* 54(12):1845–1853